AGU PUBLICATIONS

JGR

Journal of Geophysical Research: Atmospheres

RESEARCH ARTICLE

10.1002/2015JD023131

Key Points:

- Evaluation of BCC_CSM models
- Impact of horizontal resolution on model performance
- Mechanisms related to the model biases

Correspondence to:
A. Huang,
anhuang@nju.edu.cn

Citation:
Kan, M., A. Huang, Y. Zhao, Y. Zhou, B. Yang, and H. Wu (2015), Evaluation of the summer precipitation over China simulated by BCC_CSM model with different horizontal resolutions during the recent half century, *J. Geophys. Res. Atmos.*, *120*, 4657–4670, doi:10.1002/2015JD023131.

Received 21 JAN 2015
Accepted 24 APR 2015
Accepted article online 27 APR 2015
Published online 23 MAY 2015

Evaluation of the summer precipitation over China simulated by BCC_CSM model with different horizontal resolutions during the recent half century

Mengyun Kan[1], Anning Huang[1], Yong Zhao[2], Yang Zhou[1], Ben Yang[1], and Haomin Wu[3]

[1]School of Atmospheric Sciences, Nanjing University, Nanjing, China, [2]Institute of Desert Meteorology, China Meteorology Administration, Urumqi, China, [3]Lishui Meteorological Bureau, Lishui, China

Abstract The performance of Beijing Climate Center climate system model with different horizontal resolutions (BCC_CSM1.1 with coarse resolution and BCC_CSM1.1 m with fine resolution) in simulating the summer precipitation over China during the recent half century is evaluated, and the possible underlying physical mechanisms related to the model biases are also further analyzed and discussed. Results show that increasing horizontal resolution does improve the summer precipitation simulation over most part of China especially in western China due to the more realistic description of the topography. However, the summer precipitation amount (PA) over eastern China characterized by monsoonal climates is much more underestimated in the finer resolution model. It is also noted that the improvement (deterioration) of the summer PA over western (eastern) China in BCC_CSM1.1 m model is mainly due to the better (worse) simulation of the moderate and heavy precipitation relative to BCC_CSM1.1 model. In addition, increasing model horizontal resolution can significantly improve the convective precipitation simulation especially over western China but shows very limited improvement in the large-scale precipitation simulation. The much more underestimated summer PA over eastern China in BCC_CSM1.1 m model relative to BCC_CSM1.1 model is due to the significantly reduced positive biases of the convective PA but few changes in the negative biases of the large-scale PA. Further mechanism analysis suggests that both the underestimated land-sea thermal contrast and the overestimated Western Pacific subtropical high result in much less northeastward water vapor transport and summer PA over eastern China in BCC_CSM1.1 m model than in BCC_CSM1.1 model.

1. Introduction

China, located in the east of the Asian continent and on the western shore of the Pacific, is composed of a vast variety of highly different landscapes with mostly plateaus and mountains in the west and lower lands in the east (Figure 1). The terrain gradually descends from west to east like a staircase. Due to the unique distribution of topography with a vast land spanning many degrees of latitude and complex terrain, the climate over China varies radically from region to region, such as temperate continental zone over northwestern China, monsoonal climate over central and eastern China, and highland climate over Tibetan Plateau. Because the eastern seashores are affected more by the East Asian summer monsoon than inland areas in northwestern China [*Ding and Chan*, 2005], the annual rainfall is decreasing from southeast to northwest [*Gao et al.*, 2006a].

Because the inhomogeneous climates over China with great spatial variability are largely due to the heterogeneity associated with the complex terrain, growing needs to provide climate change information at fine scale usable for regional and local impact assessment have recently promoted the development of climate models with higher horizontal resolution to realistically resolve the topographical detail and simulate the climates over China [*Zhou and Li*, 2002; *Gao et al.*, 2006a; *Kusunoki et al.*, 2006; *Shi et al.*, 2008; *Gao et al.*, 2011]. Earlier studies have shown that the horizontal resolution of climate models plays an important role in simulating surface climates [*Giorgi and Mearns*, 1991; *Christensen and Kuhry*, 2000; *Gao et al.*, 2006a, 2006c], which are strongly affected by fine-scale forcing (e.g., topography and land use distribution). Recent study of *Jiang et al.* [2015] found that increasing model horizontal resolution can only improve the simulation of precipitation magnitude over land but not over the ocean and cannot significantly improve the timing of the precipitation. The sensitivity of climate models' performance to

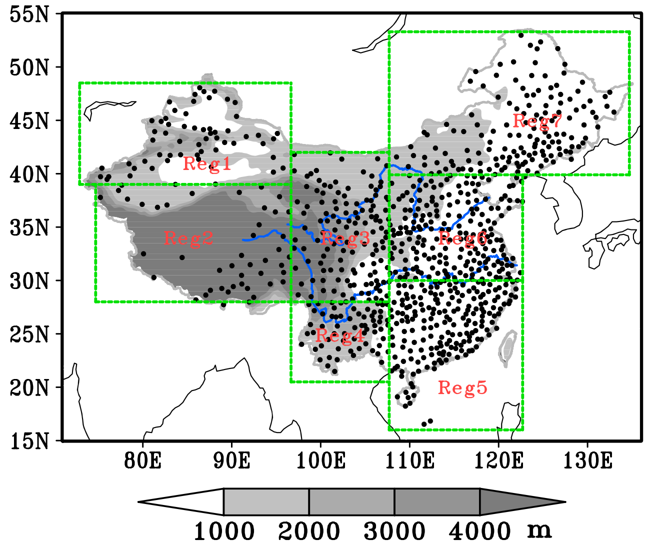

Figure 1. Distribution of the 824 observation stations (black dots) and the surface elevation (shaded). The seven subregions are denoted by green rectangles. The Yangtze River and Yellow River are indicated by blue lines.

resolution is not only due to the description of topographical detail but also to the direct sensitivity of the model physics and dynamics to resolution [*Giorgi and Marinucci*, 1996]. In addition, higher resolution helps to better simulate the fine-scale structure of synoptic and mesoscale systems which dominate the climate of a region [*Leung and Qian*, 2003; *Christensen and Kuhry*, 2000]. *Gao et al.* [2006c] indicated that model resolution plays an important role in rainfall simulation over East Asia. They also found that the small-scale weather systems are more sensitive to model resolution, and increasing model resolution can help to represent summer local convective precipitation.

Although regional climate models may apply very high resolutions [*Wang et al.*, 2000; *Gong and Wang*, 2000; *Tang et al.*, 2007; *Gao et al.*, 2006b; *Shi et al.*, 2008; *Gao et al.*, 2011], they are highly dependent upon the lateral boundary forcing, which limits their utility in studying long-term climate behaviors. Therefore, climate system models (CSMs) or coupled global climate models (CGCMs) are important tools for climate research as they can objectively describe interactions among atmosphere, hydrosphere, lithosphere, cryosphere, and biosphere in the climate systems [*Huang et al.*, 2014]. The fast growth of computer capability during the last decade has allowed a substantial increase in the resolution of CSMs or CGCMs. Indeed, long-term climate change information provided by CSMs or CGCMs with high resolution is demanded for impact assessment studies at the regional and local scales [*Tian and Jiang*, 2013]; therefore, it is very important and necessary to evaluate the performance of CSMs or CGCMs in simulating regional climates and to reveal the impacts of model resolution on climate simulation over different regions due to different applications at a wide range of spatial scales.

Previous studies have shown that most of current CSMs or CGCMs tend to display a very poor ability in simulating the climates over China [*Liang et al.*, 2001; *Rajendran et al.*, 2004; *Jiang et al.*, 2005; *Zhou and Yu*, 2006; *Ding et al.*, 2007; *Zou et al.*, 2010], especially for precipitation [*Gao et al.*, 2001, 2004; *Sun and Ding*, 2008; *Zhou et al.*, 2008a; *Xu et al.*, 2007; *Chen et al.*, 2010; *Xu and Xu*, 2012]. To realistically simulate the regional patterns, temporal variations, and correct combination of precipitation frequency (PF) and precipitation intensity (PI) is still one challenge for CSMs or CGCMs [*Kang et al.*, 2002; *Rajendran et al.*, 2004; *Wang et al.*, 2004; *Meehl et al.*, 2005; *Sun et al.*, 2006; *Zhang et al.*, 2008; *Duan et al.*, 2013].

Recently, Beijing Climate Center (BCC) of China has developed CSMs at coarse resolution (T42, or approximately 280 km; BCC_CSM1.1) and moderate resolution (T106, or approximately 110 km; BCC_CSM1.1 m), in which the ocean, land surface, atmosphere, and sea ice components are fully coupled [*Wu et al.*, 2014]. Both models have participated the Coupled Model Intercomparison Project phase five (CMIP5) experiments and contributed a large amount of simulation outputs for use in climate studies [*Xin et al.*, 2012]. Recent studies have shown that the performance of both models is comparable to that of other CMIP5 models [*Jiang et al.*, 2012; *Arora et al.*, 2013; *Su et al.*, 2013]. To reveal the performance of the BCC_CSM1.1 and BCC_CSM1.1 m models in climate simulation globally and regionally, a great number of previous studies have been conducted to address the model's ability in simulating the surface air temperature [*Gao et al.*, 2012; *Xin et al.*, 2013a, 2013b] and precipitation [*Zhang et al.*, 2013; *Su et al.*, 2013; *Wu et al.*, 2014]. The distribution of precipitation over many regions of the globe is improved in BCC_CSM1.1 m relative to BCC_CSM1.1; however, the negative precipitation bias over East Asia is increased [*Wu et al.*, 2014]. Meanwhile, both models have difficulties in reproducing the exact timing and amount of precipitation in spite of the seasonal migration of the precipitation band over East Asia captured reasonably well [*Su et al.*, 2013].

Therefore, deeply revealing the errors in simulated precipitation fields and associated influencing processes is necessary and valuable for further development and improvement of BCC_CSM model. In this study, based on the outputs of CMIP5 historical experiment produced by the BCC_CSM1.1 and BCC_CSM1.1 m models during recent half century, we focus on the evaluation of the model performance in simulating the summer precipitation over China for the reason that summer is the rainy season in China and the summer precipitation accounts for large part of the annual precipitation. Such questions will be addressed as follows: (1) How are the distributions of the summer precipitation in terms of amount, frequency, and intensity simulated by BCC_CSM1.1 and BCC_CSM1.1 m models and their biases over China? (2) Can increasing model horizontal resolution improve the summer precipitation simulation over the entire China or some subregions? (3) What are the possible physical mechanisms related to the improvement or deterioration of the precipitation simulation by increasing model horizontal resolution?

The model, data, and methodology are given in section 2. An evaluation of each model's performance in simulating the summer precipitation during the past half century is indicated in section 3. Possible underlying physical mechanisms related to the improvement or deterioration of simulation by increasing model horizontal resolution are discussed in section 4. The summary is provided in section 5.

2. Model, Data, and Methodology

2.1. Model

The CSMs used in this study are BCC_CSM1.1 and BCC_CSM1.1 m models developed by Beijing Climate Center of China. BCC_CSM1.1, adopting a horizontal resolution of T42 (or approximately 280 km) in the atmosphere and land component models [*Wu et al.*, 2014], fully couples the atmospheric model BCC_AGCM2.1 [*Huang et al.*, 2013], the land surface model BCC_AVIM1.0, the global ocean circulation model MOM4_L40v1, and the global dynamic/thermodynamic sea ice model Sea Ice Simulator (SIS) [*Winton*, 2000] using a flux coupler. The Modular Ocean Model (MOM)4_L40v1 ocean model has 40 vertical layers with a horizontal resolution of 1° × 1° poleward of 30°N and 30°S incrementally descending to 0.33° within 30°N and 30°S. The SIS sea ice model has the same horizontal resolution and sea-land distribution of the MOM4_L40v1. As the upgraded version of BCC_CSM1.1, BCC_CSM1.1 m adopts a horizontal resolution of T106 (or approximately 110 km) in the atmospheric model BCC_AGCM2.2 and land surface model BCC_AVIM1.0 with the same resolution in ocean and sea ice component models as BCC_CSM1.1 [*Wu et al.*, 2014]. Overall, both BCC_CSM1.1 and BCC_CSM1.1 m models have the same physical package and the same 26 vertical levels in atmosphere; the only difference is the horizontal resolution in the atmospheric and land surface component models.

2.2. Data

The data used in this study are listed as follows:

1. The daily precipitation, monthly convective precipitation and large-scale precipitation, and atmospheric variable outputs of the CMIP5 historical experiment [*Xin et al.*, 2013c] produced by the BCC_CSM1.1 and BCC_CSM1.1 m models during 1960–2012, which are available at http://adm07.cmcc.it/esgf-web-fe/live.
2. The daily rain gauge precipitation data (SURF_CLI_CHN_MUL_DAY_V3.0, which is available at http://cdc.cma.gov.cn/home.do) from 824 stations over China (Figure 1) during 1960 to 2012, which are collected and quality controlled by the National Meteorological Information Center of the China Meteorological Administration. As shown in Figure 1, the rain gauges are densely (coarsely) distributed in the east China (northwest China), especially rare rain gauges are located over western part of Tibetan Plateau and Tarim Basin.
3. The 40 year European Centre for Medium-Range Weather Forecasts Re-Analysis (ERA-40) monthly convective and large-scale precipitation data [*Uppala et al.*, 2005] with the horizontal resolution of 0.5° × 0.5° during 1960–2002, which is available at http://apps.ecmwf.int/datasets/data/era40_mnth/.
4. National Centers for Environmental Prediction/National Center for Atmospheric Research (NCEP/NCAR) reanalysis data [*Kalnay et al.*, 1996] during 1960–2012, including air temperature, geopotential height, and wind vectors with the horizontal resolution of 2.5° × 2.5° at 17 vertical layers, which can be obtained from ftp://ftp.cdc.noaa.gov/Datasets/ncep.reanalysis.derived/pressure/.

2.3. Methodology

The observed and modeled precipitation were interpolated onto 1° latitude × 1° longitude grid using the inverse distance weighting method [*Bartier and Keller*, 1996] within a radius of 1° around each grid box.

Based on the method provided by *Zhou et al.* [2008b], the June-July-August (JJA) averages of precipitation amount (PA) (the accumulated precipitation divided by the number of days during JJA), PF (defined as the percentage of all days during JJA having measurable precipitation above a threshold of 0.5 mm d^{-1} here), and PI (the mean rates averaged over the precipitating days) are computed for each year.

To give details of the model performance in different regions of China, China is divided into seven subregions as shown in Figure 1 with four subregions in the western China (west of 108°E), which are characterized by complex terrain and inland climates, and three subregions in eastern China, which are dominated by East Asian monsoonal climates. The seven subregions are as follows: Xinjiang (Reg.1: 73°E–97°E, 38°N–48°N), middle and western Tibetan Plateau (Reg.2: 75°E–97°E, 28°N–38°N), eastern Tibetan Plateau and Sichuan Basin (Reg.3:97°E–108°E, 28°N–42°N), Yunnan and Guizhou Plateau (Reg.4: 97°E–108°E, 20°N–28°N), southern China (Reg.5: 108°E–122°E, 16°N–30°N), Jianghuai-northern China (Reg.6: 108°E–122°E, 30°N–40°N), and northeastern China (Reg.7: 108°E–135°E, 40°N–54°N).

To quantify the model validation, a measure of skill score S [*Taylor*, 2001] for the simulated summer precipitation is given by

$$S = \frac{4(1+R)}{\left(\sigma + {}^{1}\!/_{\sigma}\right)^{2}(1+R_0)} \tag{1}$$

where R is the pattern correlation between observation and simulation, σ is the modeled spatial standard deviation divided by that of observation (so it is a normalized spatial standard deviation), and R_0 is an achievable maximum correlation (here set as 1). S evaluates both the amplitude and pattern of variability simultaneously [*Taylor*, 2001]. As the model variance approaches the observed variance (i.e., $\sigma = 1$) and as $R = R_0$, the skill approaches 1. Meanwhile, S decreases toward 0 as the correlation becomes more and more negative, or the σ approaches either zero or infinity. It is obvious that S ranges from 0 to 1 and higher skill is indicated by S with larger value. In addition, the relative errors ($RE = \frac{P_{\mathrm{model}} - P_{\mathrm{obs}}}{P_{\mathrm{obs}}} * 100\%$. P_{model} and P_{obs} are the simulation and observation, respectively), and biases are also used to evaluate the model's performance in simulating the quantity.

3. Model Evaluation

Figure 2 gives the climatology of the observed and simulated summer PA, PF, and PI. As shown in Figure 2a, the observed summer PA over China decreases from southeast to northwest. Rain band is located to the east of 95°E and stretches from the southwest to the northeast. Strong rainfall centers over 8 mm d^{-1} mainly lie in the southern China. Two large rainfall centers can also be noted over Sichuan basin and lower reaches of Yangtze River valley. Both models (Figures 2b and 2c) can reproduce the decreasing trend from southeast to northwest but produce a strong rainfall center located over the eastern Tibetan Plateau. In addition, the summer PA over the southeastern China is underestimated by both versions of BCC_CSM models. Compared to BCC_CSM1.1 model, BCC_CSM1.1 m model improves (deteriorates) the simulation of PA in the eastern Tibetan Plateau, Sichuan basin, and south coast of China (Jianghuai-northern China). Figure 2d shows that the eastern Tibetan Plateau with the observed PF over 60% rains much more frequently than the other regions of China. However, the PF in the semiarid and arid areas of northwestern China is less than 30%, especially in the Tarim basin, where the PF is below 20%. Over eastern China, the PF ranging from 30% to 60% clearly shows high-low-high centers located over southern China, Jianghuai-northern China, and northeastern China. Figures 2e and 2f show that the two models can reasonably simulate the overall observed patterns but overestimate the PF in most part of China. Compared to the BCC_CSM1.1 model, the spatial distribution of the PF produced by BCC_CSM1.1 m model is much closer to the observation. The PI (Figure 2g) shows similar features to those of PA (Figure 2a). Relative to the observation, both models underestimate the PI over eastern China (Figures 2h and 2i) with the maximum center shifting farther northwest.

Figure 3 gives the differences in the summer PA, PF, and PI between BCC_CSM1.1 simulation and observation (Figures 3a–3c) and those between BCC_CSM1.1 and BCC_CSM.1.1 m (Figures 3d–3f), respectively. From Figure 3a, the summer PA simulated by BCC_CSM1.1 model shows negative (positive) biases over north Xinjiang and southeastern China (Tarim basin, Tibetan Plateau, and Yungui Plateau) with the largest bias centers located in eastern Tibetan Plateau (over 3 mm d^{-1}) and southern China (over −2 mm d^{-1}).

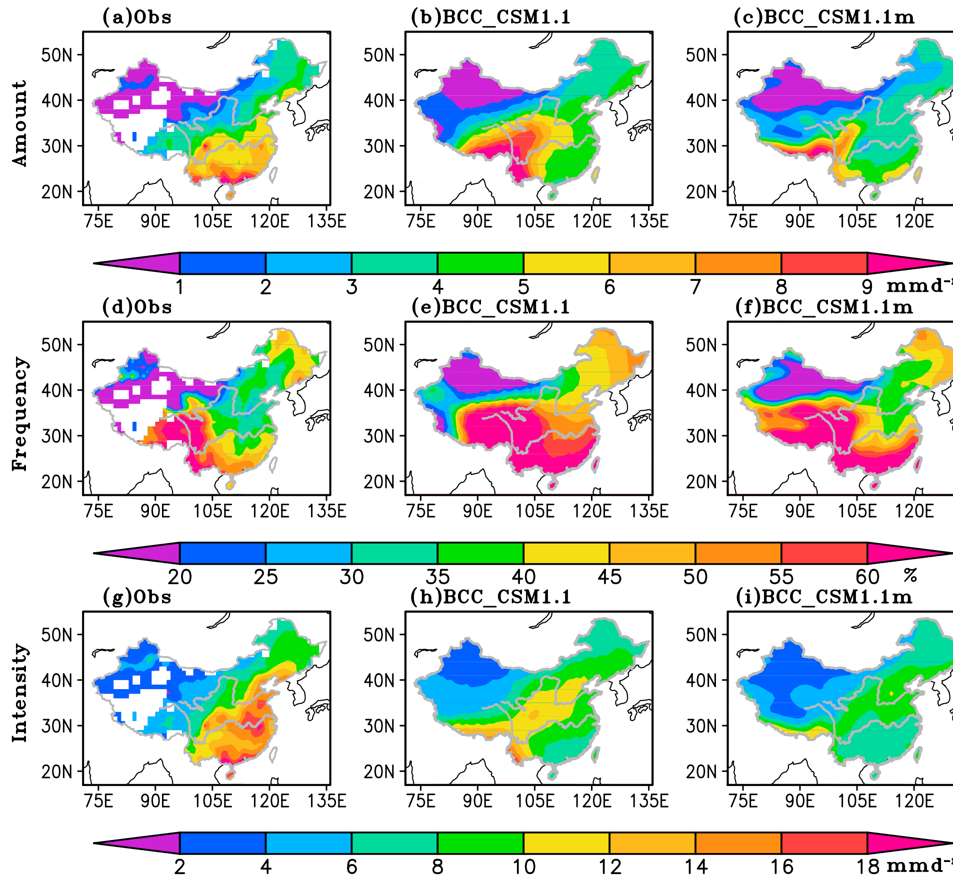

Figure 2. Spatial distributions of the observed and modeled summer mean PA, PF, and PI averaged over 1960–2012.

Compared to BCC_CSM1.1 model, the BCC_CSM1.1 m model (Figure 3d) largely reduces the biases over most of western China except for strengthened negative biases of the summer PA over most of southeastern China. It is shown in Figure 3b that the BCC_CSM1.1 model overestimates the summer PF over almost the entire China except for north Xinjiang where the summer PF is underestimated by ~5%. From Figure 3e, the biases of the modeled summer PF over most part of China in BCC_CSM1.1 m model are significantly decreased compared to BCC_CSM.1.1 model. The biases of the summer PI simulated by BCC_CSM1.1 model (Figure 3c) show similar distributions to those of summer PA (Figure 3a). Figures 3c and 3f suggest that relative to BCC_CSM1.1 model, the BCC_CSM1.1 m model improves the summer PI simulation over most part of western China; however, the negative biases over southeastern China are strengthened.

To further quantify the model performance in different subregions, the skill score *S* indicated by equation (1) and relative errors are used to evaluate the model performance in simulating both the amplitude and pattern of variability [*Taylor*, 2001] and the close agreement in quantity, respectively. As shown in Figure 4, compared with BCC_CSM1.1 model, despite the deteriorated simulation of the PA over Jianghuai-northern China (Reg.6), BCC_CSM1.1 m model improves almost all aspects of the summer precipitation climatology over China. Figure 5 exhibits the relative errors of the BCC_CSM1.1 and BCC_CSM1.1 m in simulating the climatic mean of the summer PA, PF, and PI over 1960–2012. As shown in Figures 5a and 5c, the BCC_CSM1.1 m model produces relatively smaller biases in PA and PI over western China (Regs.1–4) than BCC_CSM1.1 model. However, over eastern China which is located in East Asian summer monsoon region (Regs.5–7), the biases of the summer PA and PI are strengthened in BCC_CSM1.1 m model relative to BCC_CSM1.1 model. It is shown in Figure 5b that the biases of the simulated summer PF over all subregions in China are largely reduced by BCC_CSM1.1 m model compared to BCC_CSM1.1 model.

Overall, the results mentioned above show that BCC_CSM1.1 m model with relatively finer horizontal resolution exhibit better ability than BCC_CSM1.1 model in simulating the climatology of summer PA, PF,

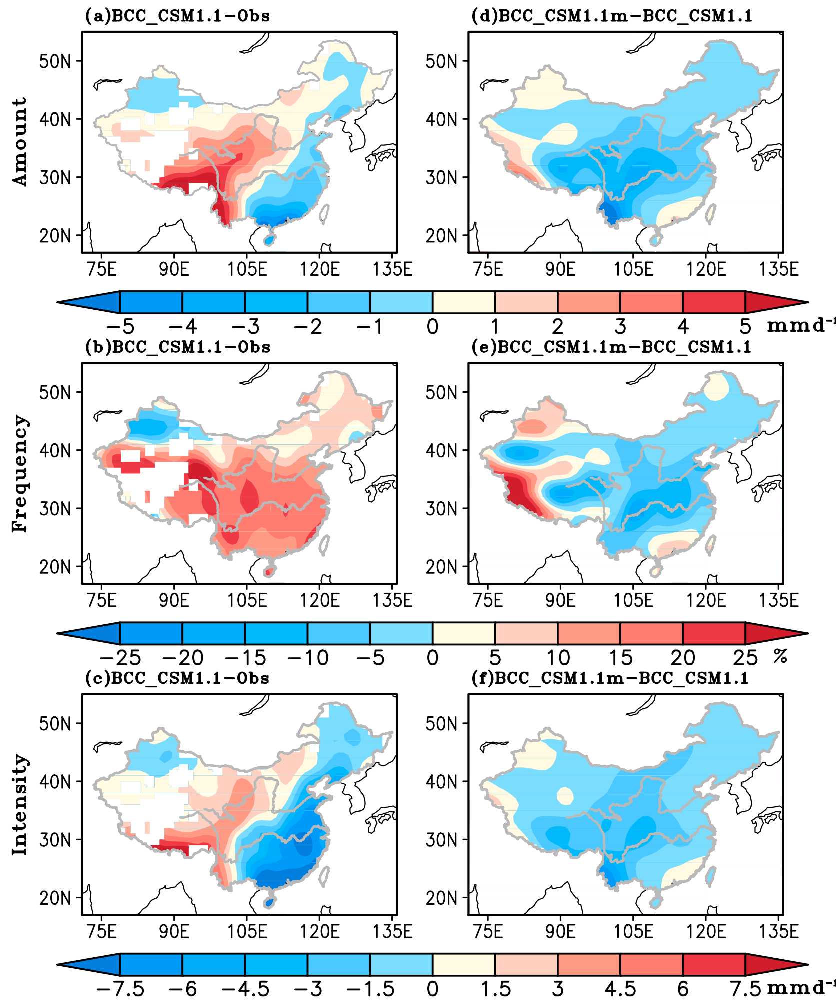

Figure 3. The spatial distributions of the differences in the summer mean PA, PF, and PI averaged over 1960–2012, respectively.

and PI over most regions of China, especially in the regions such as western China with complex terrains (Figure 1), which is possibly due to the more realistic description of the land surface in the BCC_CSM1.1 m model. Despite the improvement in simulation of both the amplitude and pattern of variability, the BCC_CSM1.1 m model shows larger biases in simulating the summer PA and PI over eastern China (Figures 5a and 5c), where the climates are largely affected by the East Asian summer monsoon.

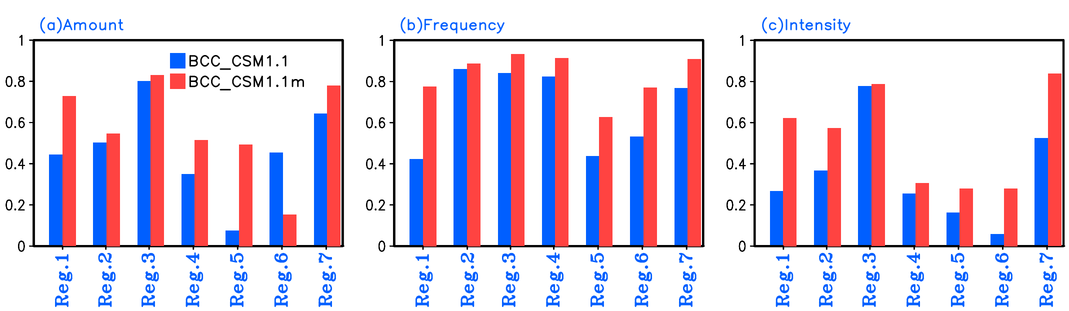

Figure 4. Scores of BCC_CSM1.1 and BCC_CSM1.1 m in simulating the climatic mean of the summer PA, PF, and PI regionally averaged over each subregion of China during 1960–2012.

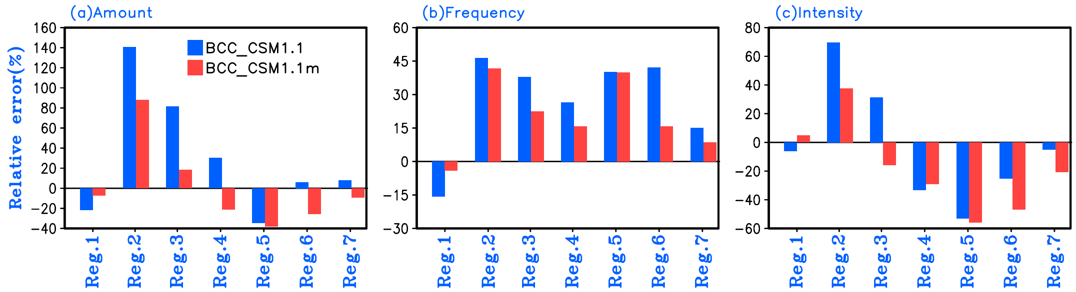

Figure 5. Relative errors of BCC_CSM1.1 and BCC_CSM1.1 m in simulating the climatic mean of the summer PA, PF, and PI regionally averaged over each subregion of China during 1960–2012.

4. Possible Causes

To further reveal what leads to the biases in the modeled summer precipitation, we first reveal the biases in different precipitation categories. According to the Chinese Central Bureau of Meteorology, precipitation is divided into four categories in terms of the daily PI as follows: light precipitation (0.1~10 mm d^{-1}), moderate precipitation (10.0~25 mm d^{-1}), heavy precipitation (25.0~50 mm d^{-1}), and torrential precipitation (≥50.0 mm d^{-1}). From the observation, over 90% of the total summer PA over northwestern China is contributed by light and moderate precipitation (Figure 6a). In contrast, the heavy and torrential precipitation contribute over 60% of the total precipitation over southeastern China in summer (Figure 6d). From the model simulations (Figures 6b, 6c, 6e, and 6f), the contributions of light and moderate precipitation to the total summer PA in both models over northwestern China are comparable to those in the observation (Figures 6a and 6d). However, the two models both overestimate (underestimate) the contributions of light and moderate (heavy and torrential) precipitation to the total PA over central and southeastern China, where the climates are strongly affected by the East Asian summer monsoon.

Figure 7 gives the differences of PA and PF for each precipitation category between the simulation of the BCC_CSM1.1 model and observation and those between BCC_CSM1.1 m and BCC_CSM1.1. From Figure 7a, the overestimated PA over Regs.2–4 in western China in BCC_CSM1.1 model are attributed to the overestimation of all precipitation categories; the underestimated (overestimated) PA in Regs.1 and 5 (Regs.6 and 7) results from the underestimated (overestimated) moderate to torrential (light and moderate) precipitation. As shown in Figure 7b, compared to BCC_CSM1.1 model, the positive biases in the summer PA over Regs.2–4 are significantly reduced, and the improved PA simulation over Regs.2 and 3 (Reg.4) is mainly due to the reduced biases in the moderate and heavy (moderate to torrential)

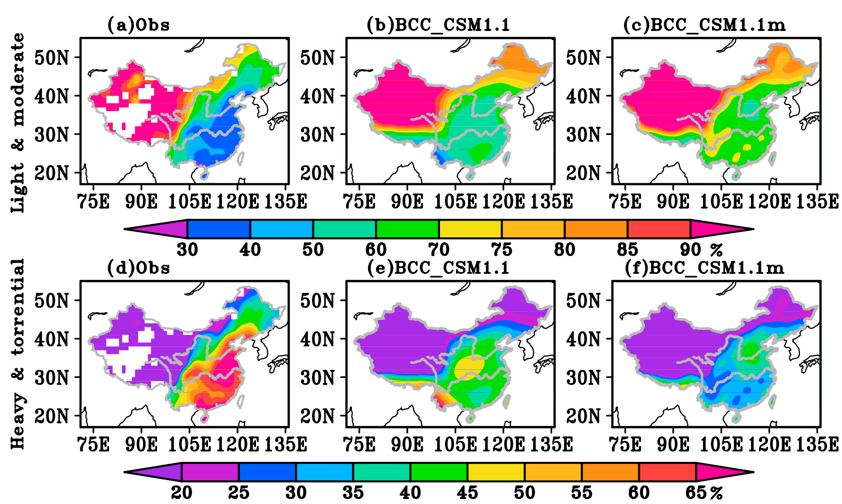

Figure 6. Distributions of the contributions of the light moderate precipitation and heavy torrential precipitation to the total summer precipitation from observation and simulation during 1960–2012.

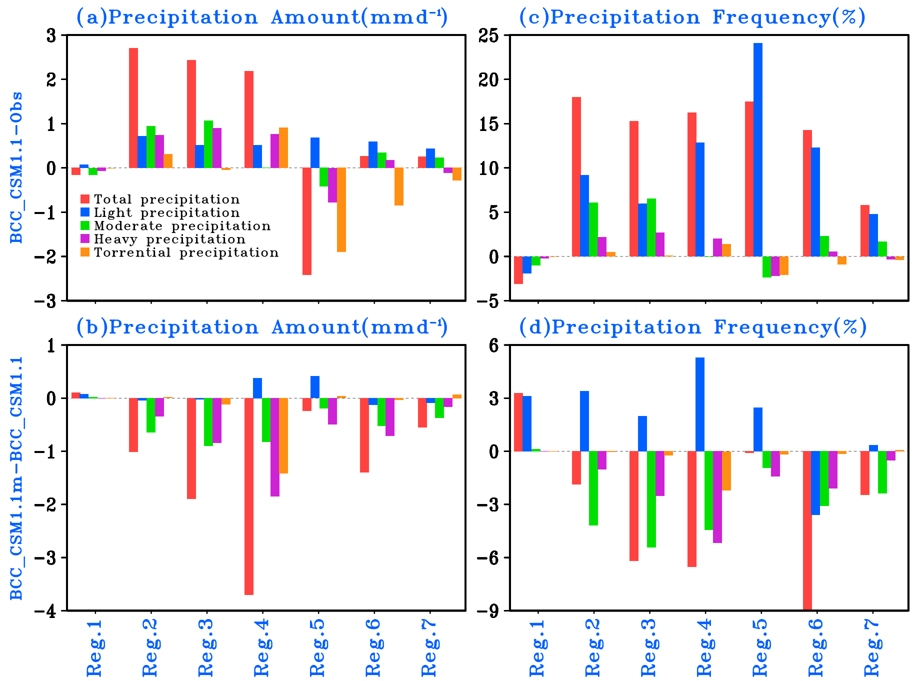

Figure 7. Differences in the climatic mean PA and PF of different precipitation categories regionally averaged over each subregion during 1960–2012.

precipitation in BCC_CSM1.1 m model. Meanwhile, BCC_CSM1.1 m model produces relatively weaker summer PA over eastern China (Regs.5–7), which is mainly attributed to the less simulated moderate and heavy precipitation.

As shown in Figure 7c, the summer PF over Regs.2–7 (Reg.1) is overestimated (underestimated) by BCC_CSM1.1 model. Among the four precipitation categories, the summer PF biases over western (eastern) China in BCC_CSM1.1 model mainly results from the biases of the light and moderate (light) PF. Relative to BCC_CSM1.1 model, the improvements of the summer PF over western China in BCC_CSM1.1 m are mainly due to the reduced biases of the moderate to heavy PF simulation (Figure 7d). However, the improved PF over eastern China in BCC_CSM1.1 m model shows much more complex features compared to those over western China. BCC_CSM1.1 m model produces more light precipitation and less moderate to torrential precipitation over southern China, while the modeled total PF is nearly unchanged relative to BCC_CSM1.1 model. The reduced biases of the light to heavy (moderate) PF result in better simulation of the total summer PF over Jianghuai-northern (northeastern) China in BCC_CSM1.1 m model than in BCC_CSM1.1 model.

As shown in Figure 8, we also present the biases of the modeled large-scale, convective, and total PA from BCC_CSM1.1 and BCC_CSM1.1 m models against ERA-40 reanalysis data over each subregion. Although some differences in the total summer PA between the ERA-40 and station gauge data can be noted (not shown), the model biases against ERA-40 data show very similar features to those relative to the station gauge data. Furthermore, the convective precipitation to total precipitation ratio in ERA-40 over China also shows very similar features to those derived from the Tropical Rainfall Measuring Mission_3A12_satellite product (not shown), indicating that the ERA-40 data can be used for model evaluation. From Figures 8a and 8b, it is noted that the convective precipitation are remarkably improved by BCC_CSM1.1 m model compared with BCC_CSM1.1 model over all subregions, especially over Regs.2–4 which are characterized by complex terrain. However, BCC_CSM1.1 m model shows very limited improvement in the large-scale precipitation relative to BCC_CSM1.1 model. BCC_CSM1.1 m model significantly improves the total PA simulation (Figure 8c) over Regs.2–4 by reducing the biases in the simulated convective precipitation compared to BCC_CSM1.1 model. However, relative to BCC_CSM1.1 model, although the biases in the convective PA is reduced over eastern China (Regs.5–7), the negative biases of the large-scale PA is not reduced, leading to an underestimation of the total PA over eastern China in BCC_CSM1.1 m model (Figure 8c).

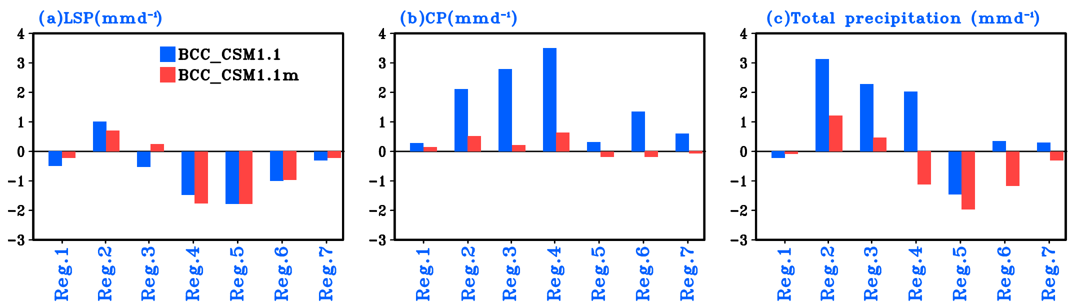

Figure 8. Model biases in the climatic summer large-scale and convective PA regionally averaged over each subregion of China during 1960–2002.

Overall, increasing model horizontal resolution can significantly improve the convective precipitation simulation over China especially over regions with complex terrain but shows very limited improvement in the large-scale precipitation simulation.

The possible mechanisms related to the atmospheric circulations leading to the biases in the precipitation simulation will be briefly discussed in the following section. To illustrate how the model horizontal resolution can affect the large-scale atmospheric circulations, Figure 9 shows the modeled and NCEP reanalysis summer geopotential height and wind vector at 850 hPa level averaged over 1960–2012. It is clearly shown in Figures 9a and 9c that BCC_CSM1.1 model produces comparable features of the geopotential height and wind vector with NCEP reanalysis. Southwesterlies can be noted along eastern

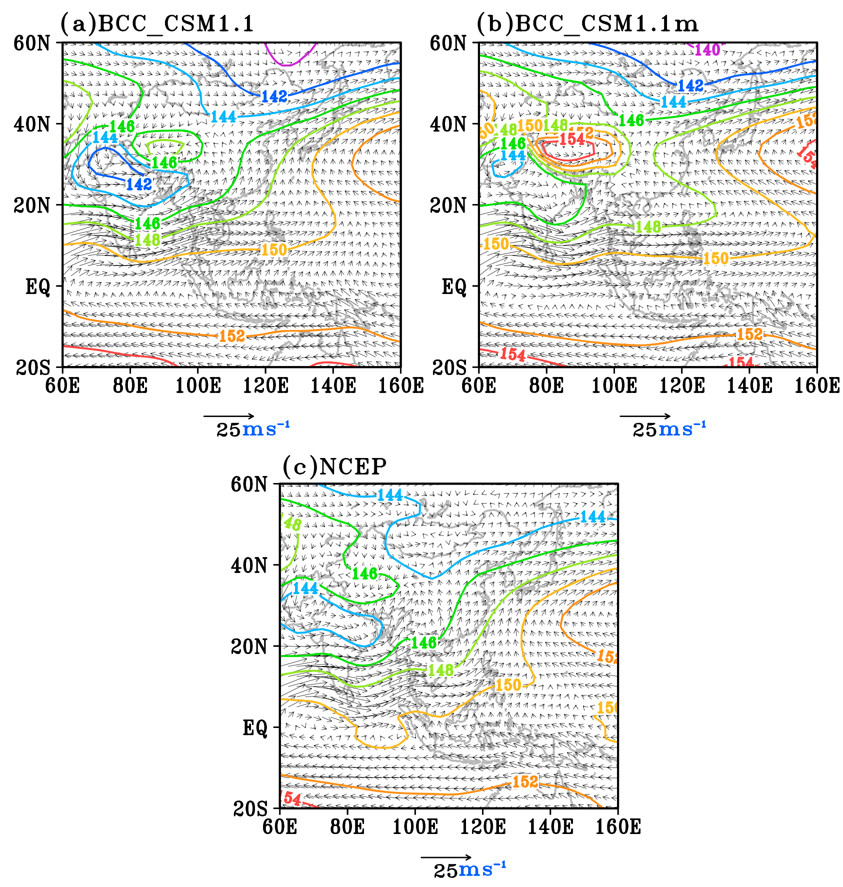

Figure 9. The modeled and NCEP reanalysis summer geopotential height (contour, dgpm) and wind vector at 850 hPa level averaged over 1960–2012.

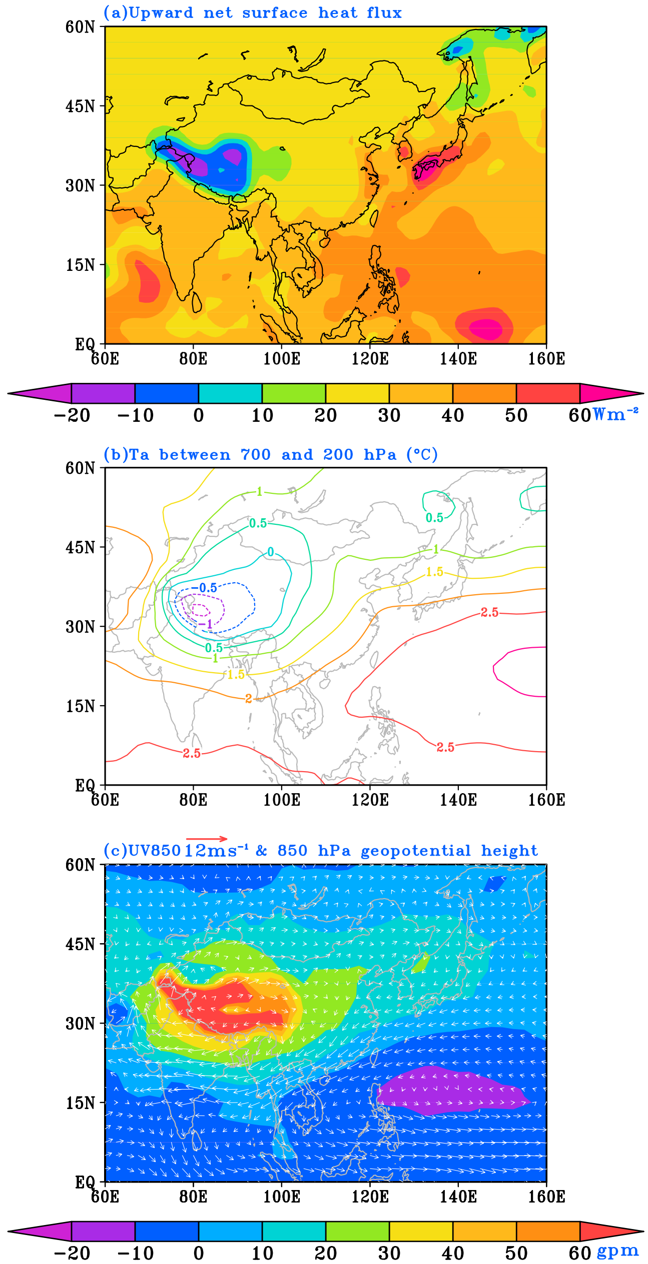

Figure 10. Differences of the summer mean (a) upward net surface heat flux, (b) vertically averaged air temperature between 700 hPa and 200 hPa, and (c) wind vector and geopotential height (shaded) at 850 hPa level between BCC_CSM1.1 m and BCC_CSM1.1 averaged over 1960–2012.

China in the simulations of the two versions of BCC_CSM model and NCEP data. However, BCC_CSM1.1 m model produced relatively weak southeasterlies over southeastern China which resulted from the overestimated Western Pacific subtropical high with farther northwest location (Figure 9b).

Figure 10 gives the differences in the summer mean upward net surface heat flux which is calculated by subtracting the sum of downward net longwave and shortwave radiation from the sum of upward sensible and latent heat fluxes, vertically averaged air temperature between 700 hPa and 200 hPa, and 850 hPa wind vector and geopotential height between BCC_CSM1.1 m and BCC_CSM1.1 simulations. As shown in Figure 10a, relative to BCC_CSM1.1 model, BCC_CSM1.1 m model produces stronger upward net surface heat flux over most part of the domain of 0°N–60°N and 60°E–160°E with large centers located over oceanic area. It can also be noted that relatively weaker upward net surface heat flux is located over Tibetan Plateau in BCC_CSM1.1 m model. The air temperature differences between 700 hPa and 200 hPa (Figure 10b) are well corresponding to the upward net surface heat flux differences (Figure 10a), resulting in weakened land-sea thermal contrast and southeast-northwestward pressure gradient force at 850 hPa level over East Asian continent and the northwest Pacific (Figure 10c). Accordingly, the southwesterlies at 850 hPa are weaker in BCC_CSM1.1 m model than in BCC_CSM1.1 model over southeastern China and adjacent oceans (Figure 10c), which will inevitably lead to the decrease of northeastward water vapor transport [*Tian et al.*, 2004; *Huang et al.*, 2007; *Zhou and Yu*, 2005] and thereafter less precipitation over southeastern China. In addition, relative to BCC_CSM1.1 model, the weakened upward net surface heat flux and lower air temperature (Figures 10a and 10b) in BCC_CSM1.1 m model could induce a stronger geopotential height center and an associated anticyclonic differences at 850 hPa level over Tibetan Plateau and adjacent regions (Figure 10c), which further weaken the southwesterlies and result in less precipitation over southeastern China in BCC_CSM1.1 m.

Figure 11 further gives the modeled and NCEP reanalysis summer geopotential height at 500 hPa level averaged over 1960–2012. Compared with BCC_CSM1.1 m model (Figure 11b), the intensity of the 500 hPa geopotential height produced by BCC_CSM1.1 model (Figure 11a) is much closer to the NCEP reanalysis

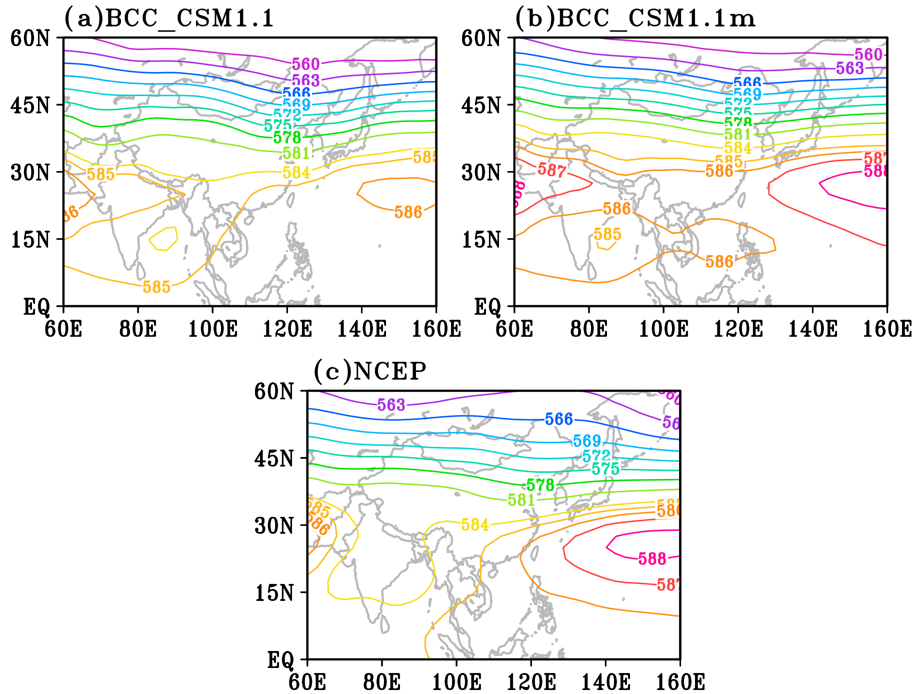

Figure 11. The modeled and NCEP reanalysis summer geopotential height at 500 hPa level averaged over 1960–2012 (unit: dgpm).

data (Figure 11c). Taking the 586 dgpm contour as reference line, we can see that BCC_CSM1.1 m model (Figure 11b) produces a much stronger subtropical high over the Western Pacific with farther northwest location, which may result in less northeastward water vapor transport (Figure 10c) and thereafter much more underestimated precipitation over southeastern China relative to BCC_CSM1.1 model (Figure 5a).

5. Concluding Remarks and Discussions

In this study, the performance of the BCC_CSM models with different horizontal resolutions (i.e., BCC_CSM1.1 and BCC_CSM1.1 m) in simulating the summer precipitation over China during 1960–2012 is evaluated. The effect of the horizontal resolution on the model performance as well as the possible reasons related to the model biases and underlying physical mechanisms are also further investigated and discussed. The main results can be obtained as follows.

BCC_CSM1.1 m model with finer horizontal resolution shows better ability than BCC_CSM1.1 model in simulating the summer precipitation amount, precipitation frequency, and precipitation intensity over most subregions of China in terms of amplitude and pattern of variability, suggesting that increasing horizontal resolution does help to improve the precipitation simulation due to more realistic description of the land surface. In addition, BCC_CSM1.1 m model reduces (increases) the biases of the PA and PI over western (eastern) China and significantly decreases the biases of the PF over all subregions of China relative to BCC_CSM1.1 model. Analysis of the biases in different precipitation categories shows that the improved simulation of PA and PF over most part of western China in BCC_CSM1.1 m model is mainly attributed to the reduced biases in the moderate and heavy precipitation. However, the much more underestimated PA over eastern China in BCC_CSM1.1 m model is mainly due to less simulated moderate and heavy PA relative to BCC_CSM1.1 model. The reduced biases of the light to heavy (moderate) PF in BCC_CSM1.1 m model result in better simulation of the total PF over Jianghuai-northern China (northeastern China) than in BCC_CSM1.1 model.

Further analysis indicates that increasing model horizontal resolution can significantly improve the convective precipitation simulation especially over regions with complex terrain but shows very limited improvement in the large-scale precipitation simulation. The significantly improved summer PA simulation over western China in BCC_CSM1.1 m model mainly results from the reduced biases of convective precipitation simulation. The much more underestimated summer PA over eastern China in BCC_CSM1.1 m model relative to BCC_CSM1.1 model is attributed to the significantly reduced positive biases of the convective PA but few changes in the negative biases of the large-scale PA. Mechanism analysis suggests that both the underestimated land-sea thermal contrast and the overestimated Western Pacific subtropical high result in much less northeastward water vapor transport and summer PA over eastern China in BCC_CSM1.1 m model than in BCC_CSM1.1 model.

This study shows that increasing horizontal resolution of BCC_CSM model can only improve the precipitation simulation over complex terrain land in western China but not over other regions, suggesting that deficiencies in model physics cannot be corrected just by increasing the horizontal resolution [*Jiang et al.*, 2015]. Both BCC_CSM1.1 m and BCC_CSM1.1 models adopt the deep convective scheme with closure assumption in which stabilization of the atmosphere by convection is in quasi-equilibrium with destabilization by large-scale forcing in the troposphere [*Wu*, 2012], implying that the precipitation intensity may be largely determined by large-scale environment which cannot be changed by just increasing horizontal resolution. This may lead to few changes in the biases of the simulated large-scale precipitation despite significant improvement of the simulated convective precipitation by increasing horizontal resolution. Meanwhile, increasing model horizontal resolution may allow more cloud processes resolved by the microphysics scheme rather than by convection scheme and result in less convective precipitation (Figure 8). In addition, increasing the atmospheric model's horizontal resolution may result in the changes of atmospheric circulation, which will affect the air-sea interaction in the coupled model system. The changed air-sea interaction in the BCC_CSM model with finer resolution may further regulate the impact of the increased horizontal resolution on the model simulation in turn [*Cherchi and Navarra*, 2007]. *Giorgi and Marinucci* [1996] have also pointed out that the sensitivity of climate models' performance to resolution is not only due to the description of topographical detail but also to the direct sensitivity of the model physics and dynamics to resolution. Since precipitation is the result of interaction among multiple atmospheric processes, such as cloud microphysics, cumulus convection, planetary boundary layer processes, and many others, studies on the sensitivity of the model dynamics and different physical processes to horizontal resolution are needed in the future to further improve the precipitation simulation over the East Asian monsoon regions.

Acknowledgments
This work was supported by the National Natural Science Foundation of China under grants 41175086 and 41275076, the Special Program for China Meteorology Trade under grant GYHY201306020, and the Jiangsu Collaborative Innovation Center for Climate Change. We are grateful to NCEP/NCAR (ftp://ftp.cdc.noaa.gov/Datasets/ncep.reanalysis.derived/pressure/) and ECMWF (http://apps.ecmwf.int/datasets/data/era40_mnth/) for allowing us to use the reanalysis data. We thank National Meteorological Information Center of the China Meteorological Administration for providing the gauge observed precipitation data (SURF_CLI_CHN_MUL_DAY_V3.0 which is available at http://cdc.cma.gov.cn/home.do). We also acknowledge the World Climate Research Programme's Working Group on Coupled Modeling which is responsible for CMIP5 making the outputs of BCC_CSM models available at http://adm07.cmcc.it/esgf-web-fe/live.

References

Arora, V., et al. (2013), Carbon concentration and carbon-climate feedback in CMIP5 Earth system models, *J. Clim.*, *26*, 5289–5314, doi:10.1175/JCLI-D-12-00494.1.

Bartier, P. M., and C. P. Keller (1996), Multivariate interpolation to incorporate thematic surface data using inverse distance weighting (IDW), *C. R. Geosci.*, *22*(7), 795–799, doi:10.1016/0098-3004(96)00021-0.

Chen, H., T. Zhou, R. B. Neale, X. Wu, and G. J. Zhang (2010), Performance of the new NCAR CAM3.5 model in East Asian summer monsoon simulations: Sensitivity to modifications of the convection scheme, *J. Clim.*, *23*, 3657–3675.

Cherchi, A., and A. Navarra (2007), Sensitivity of the Asian summer monsoon to the horizontal resolution: differences between AMIP-type and coupled model experiments, *Clim. Dyn.*, *28*, 273–290.

Christensen, J. H., and P. Kuhry (2000), High resolution regional climate model validation and permafrost simulation for the East European Russian Arctic, *J. Geophys. Res.*, *105*, 29,647–29,658, doi:10.1029/2000JD900379.

Ding, Y., and J. C. L. Chan (2005), The East Asian summer monsoon: An overview, *Meteorol. Atmos. Phys.*, *89*, 117–142.

Ding, Y., G. Ren, Z. Zhao, Y. Xu, Y. Luo, Q. Li, and J. Zhang (2007), Detection, causes and projection of climate change over China: An overview of recent progress, *Adv. Atmos. Sci.*, *24*, 954–971.

Duan, A., J. Hu, and Z. Xiao (2013), The Tibetan Plateau summer monsoon in the CMIP5 simulations, *J. Clim.*, *26*, 7747–7766.

Gao, F., X. Xin, and T. Wu (2012), A study of the prediction of regional and global temperature on decadal time scale with BCC_CSM1.1 model [in Chinese], *Chin. J. Atmos. Sci.*, *36*(6), 1165–1179.

Gao, X., Z. Zhao, Y. Ding, R. Huang, and F. Giorgi (2001), Climate change due to greenhouse effects in China as simulated by a regional climate model, *Adv. Atmos. Sci.*, *18*, 1224–1230.

Gao, X., W. Lin, F. Kucharsky, and C. Zhao (2004), A simulation of regional climate in China by using CCM3 and observed SST [in Chinese], *Chin. J. Atmos. Sci.*, *28*, 78–90.

Gao, X., Y. Xu, Z. Zhao, J. Pao, and F. Giorgi (2006a), On the role of resolution and topography in the simulation of East Asia precipitation, *Theor. Appl. Climatol.*, *86*, 173–185.

Gao, X., J. S. Pal, and F. Giorgi (2006b), Projected changes in mean and extreme precipitation over the Mediterranean region from a high resolution double nested RCM simulation, *Geophys. Res. Lett.*, *33*, L03706, doi:10.1029/2005GL024954.

Gao, X., Y. Xu, and Z. Zhao (2006c), Impacts of horizontal resolution and topography on the numerical simulation of East Asian precipitation [in Chinese], *Chin. J. Atmos. Sci.*, *30*(2), 185–192.

Gao, X., Y. Shi, and G. Filippo (2011), A high resolution simulation of climate change over China, *Sci. China Earth Sci.*, *54*(3), 462–472.

Giorgi, F., and M. Marinucci (1996), Improvements in the simulation of surface climatology over the European region with a nested modeling system, *Geophys. Res. Lett.*, *23*, 273–276, doi:10.1029/96GL00050.

Giorgi, F., and L. O. Mearns (1991), Approaches to regional climate change simulations: A review, *Rev. Geophys.*, *29*, 191–216, doi:10.1029/90RG02636.

Gong, W., and W. Wang (2000), A regional model simulation of the 1991 severe precipitation event over the Yangtze-Huai river Valley: Part II: model bias, *J. Clim.*, *13*, 93–108.

Huang, A., Y. Zhang, and X. Gao (2007), Impacts of coastal SST variability on the East Asian summer monsoon, *Adv. Atmos. Sci.*, *24*, 259–270.

Huang, A., et al. (2013), Extended range simulations of the extreme snow storms over southern China in early 2008 with the BCC_AGCM2.1 model, *J. Geophys. Res. Atmos.*, *118*, 8253–8273, doi:10.1002/jgrd.50638.

Huang, A., Y. Zhou, Y. Zhang, D. Huang, Y. Zhao, and H. Wu (2014), Changes of the annual precipitation over central Asia in the twenty-first century projected by multimodels of CMIP5, *J. Clim.*, *27*, 6627–6646.

Jiang, D., H. Wang, and X. Lang (2005), Evaluation of East Asian climatology as simulated by seven coupled models, *Adv. Atmos. Sci.*, *22*(4), 479–495.

Jiang, J. H., et al. (2012), Evaluation of cloud and water vapor simulations in CMIP5 climate models using NASA "A-Train" satellite observations, *J. Geophys. Res.*, *117*, D14105, doi:10.1029/2011JD017237.

Jiang, J. H., et al. (2015), Evaluating the diurnal cycle of upper tropospheric ice clouds in climate models using SMILES observations, *J. Atmos. Sci.*, *72*(3), 1022–1044.

Kalnay, E., et al. (1996), The NCEP/NCAR 40-year reanalysis project, *Bull. Am. Meteorol. Soc.*, *77*(3), 437–471.

Kang, I., et al. (2002), Intercomparison of the climatological variations of Asian summer monsoon precipitation simulated by 10 GCMs, *Clim. Dyn.*, *19*, 383–395.

Kusunoki, S., J. Yoshemeura, H. Yoshimura, A. Noda, K. Oouchi, and R. Mizuta (2006), Change of Baiu rainband in global warming projection by an atmospheric general circulation model with a 20-km grid size, *J. Meteorol. Soc. Jpn.*, *84*, 581–611.

Leung, L., and Y. Qian (2003), The sensitivity of precipitation and snowpack simulations to model resolution via nesting in regions of complex terrain, *J. Hydrometeorol.*, *4*, 1025–1043.

Liang, X., W. Wang, and A. Samel (2001), Biases in AMIP model simulations of the east China monsoon system, *Clim. Dyn.*, *17*, 291–304.

Meehl, G. A., C. Covey, B. McAvaney, M. Latif, and R. J. Stouffer (2005), Overview of the Coupled Model Intercomparison Project, *Bull. Am. Meteorol. Soc.*, *86*, 89–93.

Rajendran, K., A. Kitoh, and S. Yukimoto (2004), South and East Asian summer monsoon climate and variation in the MRI coupled model (MRI-CGCM2), *J. Clim.*, *17*, 763–782.

Shi, X., Y. Wang, and X. Xu (2008), Effect of mesoscale topography over the Tibetan Plateau on summer precipitation in China: A regional model study, *Geophys. Res. Lett.*, *35*, L19707, doi:10.1029/2008GL034740.

Su, H., et al. (2013), Diagnosis of regime-dependent cloud simulation errors in CMIP5 models using "A-Train" satellite observations and reanalysis data, *J. Geophys. Res. Atmos.*, *118*, 2762–2780, doi:10.1029/2012JD018575.

Sun, Y., and Y. Ding (2008), An assessment on the performance of IPCC AR4 climate models in simulating interdecadal variations of the East Asian summer monsoon, *Acta Meteorol. Sin.*, *22*, 472–488.

Sun, Y., S. Solomon, A. Dai, and R. W. Portmann (2006), How often does it rain?, *J. Clim.*, *19*(6), 916–934.

Tang, J., M. Zhao, and B. Su (2007), The Effects of model resolution on the simulation of regional climate extreme events, *Acta Meteorol. Sin.*, *21*(1), 129–140.

Taylor, K. E. (2001), Summarizing multiple aspects of model performance in a single diagram, *J. Geophys. Res.*, *106*, 7183–7192, doi:10.1029/2000JD900719.

Tian, H., P. Guo, and W. Lu (2004), Characteristics of vapor inflow corridors related to summer rainfall in China and impact factors [in Chinese], *J. Trop. Meteorol.*, *20*(4), 401–408.

Tian, Z., and D. Jiang (2013), Evaluation of the performance of low- to high-resolution CCSM4 over East Asia and China [in Chinese], *Chin. J. Atmos. Sci.*, *37*(1), 171–186.

Uppala, S. M., et al. (2005), The ERA-40 Re-Analysis, *Q. J. R. Meteorol. Soc.*, *131*, 2961–3012.

Wang, B., I. S. Kang, and J. Y. Lee (2004), Ensemble simulations of Asian-Australian monsoon variability by 11 AGCMs, *J. Clim.*, *17*(4), 803–818.

Wang, W., W. Gong, and H. Wei (2000), A regional model simulation of the 1991 severe precipitation event over the Yangtze-Huai River Valley: Part I: Precipitation and circulation statistics, *J. Clim.*, *13*, 74–92.

Winton, M. (2000), A reformulated three-layer sea ice model, *J. Atmos. Oceanic Technol.*, *17*, 525–531.

Wu, T. (2012), A mass-flux cumulus parameterization scheme for large-scale models: Description and test with observations, *Clim. Dyn.*, *38*, 725–744, doi:10.1007/s00382-011-0995-3.

Wu, T., et al. (2014), An overview of BCC climate system model development and application for climate change studies, *J. Meteorol. Res.*, *1*, 34–56.

Xin, X., T. Wu, and J. Zhang (2012), Introduction of CMIP5 experiments carried out by BCC climate system model [in Chinese], *Adv. Clim. Change Res.*, *8*, 378–382.

Xin, X., T. Wu, J. Li, Z. Wang, W. Li, and F. Wu (2013a), How well does BCC_CSM1.1 reproduce the 20th century climate change over China?, *Atmos. Oceanic. Sci. Lett.*, *6*, 21–26.

Xin, X., L. Zhang, J. Zhang, T. Wu, and Y. Fang (2013b), Climate change projections over East Asia with BCC_CSM1.1, climate model under RCP scenarios, *J. Meteorol. Soc. Jpn.*, *91*(4), 413–429.

Xin, X., T. Wu, and J. Zhang (2013c), Introduction of CMIP5 experiments carried out with the climate system models of Beijing Climate Center [in Chinese], *Adv. Clim. Change Res.*, *4*, 41–49.

Xu, C., X. Shen, and Y. Xu (2007), An analysis of climate change in East Asia by using the IPCC AR4 simulations [in Chinese], *Adv. Clim. Change Res.*, *3*(5), 287–292.

Xu, Y., and C. Xu (2012), Preliminary assessment of simulations of climate changes over China by CMIP5 multimodels, *Atmos. Oceanic Sci. Lett.*, *5*, 489–494.

Zhang, L., Y. Ding, and Y. Sun (2008), Evaluation of precipitation simulation in East Asian monsoon areas by coupled ocean-atmosphere general circulation models [in Chinese], *Chin. J. Atmos. Sci.*, *32*(2), 261–276.

Zhang, L., T. Wu, and X. Xin (2013), The annual modes of tropical precipitation simulated by Beijing Climate Center climate system model (BCC_CSM) [in Chinese], *Chin. J. Atmos. Sci.*, *37*(5), 994–1012.

Zhou, T., and Z. Li (2002), Simulation of the East Asian summer monsoon using a variable resolution atmospheric GCM, *Clim. Dyn.*, *19*, 167–180.

Zhou, T., and R. Yu (2005), Atmospheric water vapor transport associated with typical anomalous summer rainfall patterns in China, *J. Geophys. Res.*, *110*, D08104, doi:10.1029/2004JD005413.

10.1002/2015JD023131

Zhou, T., and R. Yu (2006), Twentieth-century surface air temperature over China and the globe simulated by coupled climate models, *J. Clim.*, *19*, 5843–5858.
Zhou, T., R. Yu, H. Li, and B. Wang (2008a), Ocean forcing to changes in global monsoon precipitation over the recent half-century, *J. Clim.*, *21*, 3833–3852.
Zhou, T., R. Yu, H. Chen, A. Dai, and Y. Pan (2008b), Summer precipitation frequency, intensity, and diurnal cycle over China: A comparison of satellite data with rain gauge observations, *J. Clim.*, *21*, 3997–4010.
Zou, L., T. Zhou, L. Laurent, and J. Zhang (2010), East China summer rainfall variability of 1958–2000: Dynamical downscaling with a variable-resolution AGCM, *J. Clim.*, *23*, 6394–6408.